nature medicine

Endothelial-to-mesenchymal transition contributes to cardiac fibrosis

Elisabeth M Zeisberg[1], Oleg Tarnavski[2], Michael Zeisberg[1], Adam L Dorfman[3], Julie R McMullen[4], Erika Gustafsson[5], Anil Chandraker[6], Xueli Yuan[6], William T Pu[3], Anita B Roberts[7], Eric G Neilson[8], Mohamed H Sayegh[6], Seigo Izumo[2] & Raghu Kalluri[1,9,10]

Cardiac fibrosis, associated with a decreased extent of microvasculature and with disruption of normal myocardial structures, results from excessive deposition of extracellular matrix, which is mediated by the recruitment of fibroblasts. The source of these fibroblasts is unclear and specific anti-fibrotic therapies are not currently available. Here we show that cardiac fibrosis is associated with the emergence of fibroblasts originating from endothelial cells, suggesting an endothelial-mesenchymal transition (EndMT) similar to events that occur during formation of the atrioventricular cushion in the embryonic heart. Transforming growth factor-β1 (TGF-β1) induced endothelial cells to undergo EndMT, whereas bone morphogenic protein 7 (BMP-7) preserved the endothelial phenotype. The systemic administration of recombinant human BMP-7 (rhBMP-7) significantly inhibited EndMT and the progression of cardiac fibrosis in mouse models of pressure overload and chronic allograft rejection. Our findings show that EndMT contributes to the progression of cardiac fibrosis and that rhBMP-7 can be used to inhibit EndMT and to intervene in the progression of chronic heart disease associated with fibrosis.

Diastolic dysfunction associated with preserved systolic function is increasingly recognized as an important cause of heart failure[1–3]. An underlying morphological correlate of diastolic dysfunction is cardiac fibrosis, which leads to increased stiffness of the heart[3]. Moreover, fibrosis in the heart is a common feature in patients with advanced cardiac failure, regardless of the etiology of cardiomyopathy. Specific anti-fibrotic therapies are not currently available in the clinic[3]. Cardiac fibrosis is associated with the disruption of normal myocardial structure through excessive deposition of extracellular matrix (ECM)[3]. Fibrosis in the heart seems to follow a similar pathway as fibrosis in other epithelial organs, such as the liver, kidney, lung, skin and solid tumors[4]. As in other organs, the predominant cellular mediators of fibrosis in the heart are thought to be fibroblasts[4]. However, the origin of such fibroblasts in the adult heart is unclear.

Traditionally, adult fibroblasts are considered to be derived directly from embryonic mesenchymal cells[5,6] and to increase in number solely as a result of the proliferation of resident fibroblasts[4]. However, recent studies in organs such as the kidney, lung and liver and in metastatic tumors have shown that during fibrosis, in addition to the proliferation of resident fibroblasts, bone marrow–derived fibroblasts and epithelial cells contribute to fibroblast accumulation through an epithelial-mesenchymal transition (EMT)[7].

Endothelial-mesenchymal transition (EndMT) is a form of EMT that occurs during the embryonic development of the heart: the mesenchymal cells that form the atrioventricular cushion, the primordia of the valves and septa of the adult heart, are derived from the endocardium by EndMT[8]. This process occurs in the outflow tract and the atrioventricular canal in a spatiotemporally restricted manner, and is thought to be initiated by inductive signals such as TGF-β and BMPs from the myocardium[9–14]. Because some forms of heart fibrosis are predominantly characterized by a perivascular and subendocardial fibrosis, we hypothesized that during cardiac fibrosis, EndMT might contribute to the accumulation of cardiac fibroblasts, recapitulating pathways associated with cardiac development.

Here we use *Tie1Cre;R26RstoplacZ* mice, in which cells of endothelial origin are irrevocably marked by *lacZ* expression, and *FSP1-GFP* transgenic mice, in which green fluorescent protein (GFP) is expressed under the control of the promoter of fibroblast-specific protein 1 (FSP1). We show that, during cardiac fibrosis, endothelial cells undergo EndMT and contribute to the total pool of cardiac fibroblasts, as observed during formation of the atrioventricular cushion[15,16]. To our knowledge, EndMT has not been previously described in any adult tissue. TGF-β1, a promoter of cardiac fibrosis, induced EndMT in adult coronary endothelial cells, whereas rhBMP-7 preserved the

[1]Division of Matrix Biology, Department of Medicine, Beth Israel Deaconess Medical Center & Harvard Medical School, Boston, Massachusetts 02215, USA. [2]Novartis Institute for Biomedical Research, Cambridge, Massachusetts 02139, USA. [3]Department of Cardiology, Children's Hospital, Boston, Massachusetts 02115, USA. [4]Cardiovascular Division, Department of Medicine, Department of Cardiology, Beth Israel Deaconess Medical Center & Harvard Medical School, Boston, Massachusetts 02215, USA. [5]Department of Experimental Pathology, Lund University, 22185 Lund, Sweden. [6]Transplantation Research Center, Brigham and Women's Hospital & Children's Hospital, Boston, Massachusetts 02215, USA. [7]Laboratory of Cell Regulation and Carcinogenesis, National Cancer Institute, National Institutes of Health, Bethesda, Maryland 20892, USA. [8]Department of Medicine, Vanderbilt University, Nashville, Tennessee 37215, USA. [9]Department of Biological Chemistry and Molecular Pharmacology, Harvard Medical School, Boston, Massachusetts 02215, USA. [10]Harvard-MIT Division of Health Sciences and Technology, Boston, Massachusetts 02215, USA. Correspondence should be addressed to R.K. (rkalluri@bidmc.harvard.edu).

Received 29 January; accepted 1 June; published online 29 July 2007; doi:10.1038/nm1613

endothelial phenotype and reversed TGF-β1–induced EndMT. TGF-β1–induced cardiac fibrosis was impaired in mice heterozygous for the transcription factor Smad3, which is involved in TGF-β1 signaling. This result further implicates TGF-β1 signaling in the pathogenesis of cardiac fibrosis. In two models of cardiac fibrosis, systemic administration of rhBMP-7 caused a significant reduction in the number of fibroblasts and in the amount of ECM observed, in association with an improvement in heart function. The reduction of fibrosis by rhBMP-7 was associated with a specific reduction in the number of fibroblasts carrying an endothelial imprint, indicating that rhBMP-7 can inhibit EndMT in the heart.

RESULTS

EndMT in cardiac fibrosis

To examine whether EndMT occurs during cardiac fibrosis, we performed lineage analysis of fibroblasts recruited during fibrosis using *Tie1Cre;R26RstoplacZ* double-transgenic mice (**Fig. 1a**)[15,16]. The *Tie1* gene encodes a tyrosine kinase receptor that is expressed by endothelial cells of all organs, from early in vascular development throughout adulthood[15,17]. In *Tie1Cre* mice, expression of the Cre recombinase is controlled by the *Tie1* promoter and thus Cre is expressed in endothelial cells. In the *R26RstoplacZ* indicator strain, the *lacZ* reporter gene is expressed upon Cre-mediated excision of a *loxP* stop cassette. Therefore, in the *Tie1Cre;R26RstoplacZ* double-transgenic mice, *lacZ* gene expression persists in cells of endothelial origin, despite any subsequent phenotypic alterations.

To investigate the contribution of EndMT to cardiac fibrosis, we performed aortic banding in *Tie1Cre;R26RstoplacZ* adult mice. In normal hearts, *lacZ* expression (as detected by staining for β-galactosidase (β-gal) activity) could be detected only in blood vessel–associated endothelial cells (**Fig. 1b**). In the hearts of banded mice, *lacZ*-positive cells were scattered throughout the fibrotic area

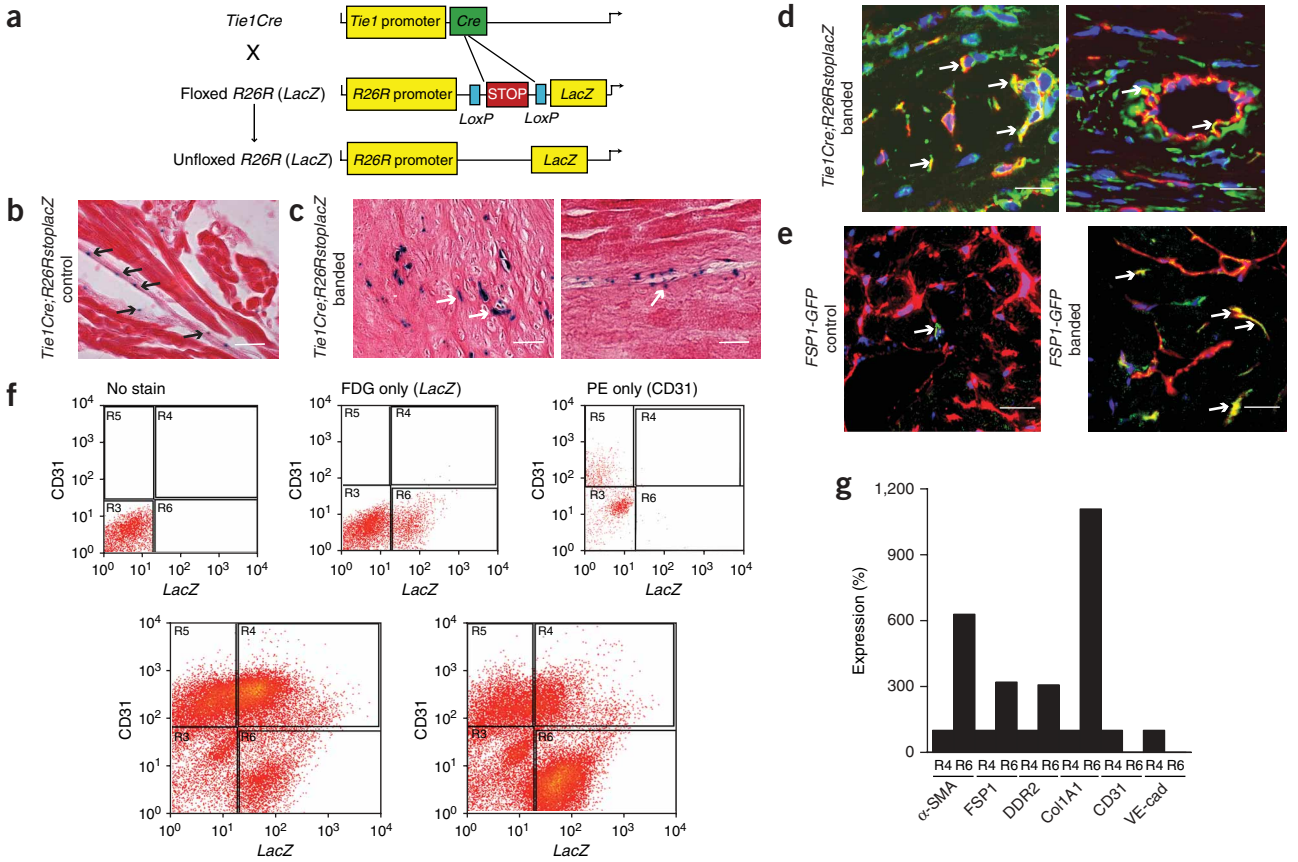

Figure 1 Lineage tracing of EndMT in *Tie1Cre;R26RstoplacZ* mice. (**a**) Gene constructs present in *Tie1Cre;R26RstoplacZ* mice. (**b**) An example of an unbanded control heart, in which *lacZ* expression was detected only in vessels (blue staining, arrows; eosin counterstain, red). (**c**) Representative sections of a banded heart, where *lacZ* expression was detected throughout the fibrotic tissue (arrows). The arrow in the right picture points to a blue cell directly adjacent to a vessel. (**d**) Confocal immunofluorescence double-labeling in banded *Tie1Cre;R26RstoplacZ* hearts with antibodies to β-gal (red) and FSP1 (green). Arrows, colocalization of β-gal and FSP1 expression involving both microvessels (left) and arterioles (right). (**e**) Normal unbanded control hearts and hearts of banded FSP1–GFP mice were stained for GFP (green) and CD31 (red). Confocal microscopy revealed GFP expression in few fibroblasts (GFP^+CD31^- cells) in normal hearts (left, arrow points to a GFP^+CD31^- cell). In banded hearts, GFP^+ endothelial cells co-expressed GFP and CD31 (right; arrows point to GFP^+CD31^+ cells). Nuclei were counterstained with TOPRO-3 (blue). (**f**) Single cells from unbanded and banded *Tie1Cre;R26RstoplacZ* mice were FACS sorted according to *lacZ* and CD31 expression. Top, negative and positive controls (from a heart from *Rosa26* mice, in which all cells express *lacZ*). *LacZ* activity was detected with FDG-green (*x* axis); CD31 protein was labeled with PE-red (*y* axis). In normal hearts (bottom left), $lacZ^+CD31^+$ cells were most prominent (gate R4). This population was decreased in fibrotic hearts (bottom right) in favor of $lacZ^+CD31^-$cells (gate R6). (**g**) Cells from gates R4 and R6 of two banded *Tie1Cre;R26RstoplacZ* hearts were sorted and compared by real-time PCR. Expression of mRNAs encoding the mesenchymal markers α-SMA, FSP1, DDR-2 and collagen I α1 (Col1A1) in the $lacZ^+CD31^-$ (R6) cell population of banded hearts is shown compared with their expression in the $lacZ^+CD31^+$ (R4) cell population. Scale bars, 20 μm.

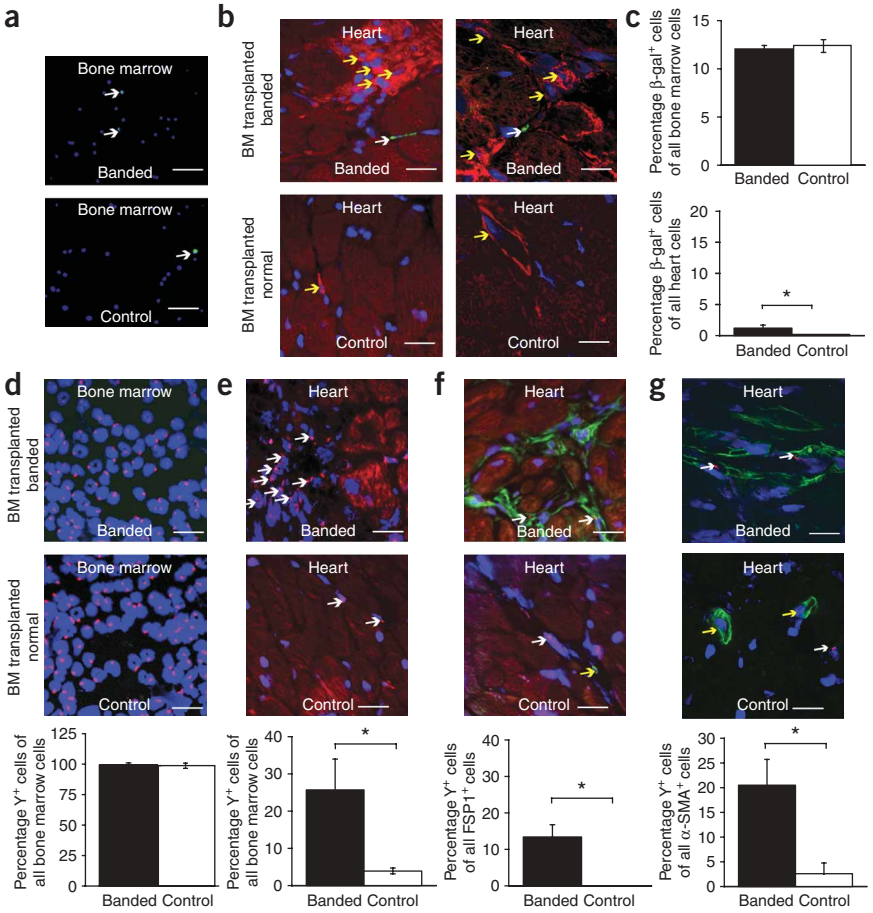

Figure 2 Bone marrow–derived Tie1$^+$ cells in cardiac fibrosis. (**a–c**) Aortic banding was performed in wild-type mice 3 weeks after bone marrow transplantation from *Tie1Cre; R26RstoplacZ* mice and the contribution of bone marrow–derived cells to Tie1$^+$ fibroblasts was assessed. Control, unbanded hearts. (**a**) Detection of bone marrow cells with antibodies to β-gal (green) confirmed the presence of Tie1-expressing progenitor cells (arrows) in the bone marrow of banded (top) and unbanded (bottom) transplanted mice. Scale bars, 100 μm. (**b**) In banded hearts (top), few β-gal$^+$ cells (green) were detected in vessels (white arrows). β-gal$^+$ cells were not detected outside the vascular compartment and did not colocalize with FSP1$^+$ cells (red, top and bottom left, yellow arrows). In unbanded hearts (bottom left) no β-gal$^+$ cells could be detected. Double labeling with antibodies to β-gal (green) and α-SMA (red, top and bottom right) revealed that (bone marrow–derived) β-gal$^+$ cells did not colocalize with α-SMA (bottom right, α-SMA$^+$ cells are indicated by yellow arrows). Scale bars, 20 μm. (**c**) Quantification of β-gal$^+$ cells in the bone marrow (top) and hearts (bottom) of mice that received bone marrow transplantation from *Tie1Cre;R26RstoplacZ* mice. $n = 3$ mice per group. Control, unbanded hearts. (**d–g**) Female wild-type mice were transplanted with male bone marrow, and aortic banding was performed 3 weeks later. Control, unbanded hearts. Hearts and bone marrow were analyzed by FISH for the Y chromosome (red dots in nuclei, white arrows). Scale bars, 20 μm. (**d**) Detection of Y chromosomes in the bone marrow confirmed the complete reconstitution of the bone marrow by male donor cells. (**e**) In banded hearts, many cells carrying a Y chromosome could be detected in fibrotic areas (top, white arrows); in normal hearts only few bone marrow–derived cells were present (bottom). (**f**) Simultaneous FISH for the Y chromosome and immunostaining for FSP1 (FITC-green) showed a subpopulation of FSP1$^+$, bone marrow–derived fibroblasts in fibrotic hearts (top, white arrows). In normal hearts none of the FSP1$^+$ cells (bottom, yellow arrow) carried a Y chromosome. White arrow (bottom panel), FSP1$^-$ cell with a Y chromosome. (**g**) Simultaneous FISH for the Y chromosome and immunostaining for α-SMA (FITC-green) revealed bone marrow–derived, α-SMA$^+$ fibroblasts in fibrotic hearts (top, white arrows). In normal hearts, bone marrow–derived, α-SMA$^+$ fibroblasts were rare (bottom, yellow arrows indicate α-SMA$^+$ fibroblasts, white arrow indicates a Y-chromosome$^+$ cell). Nuclei were counterstained with TOPRO-3 (blue). For the quantitative results shown in **d–g**, $n = 3$ mice per group. Control, unbanded hearts.* $P \leq 0.05$.

(**Fig. 1c**). To provide evidence that these scattered *lacZ*-positive cells are mesenchymal cells of endothelial origin, we performed immunofluorescence double-labeling experiments using antibodies to β-gal (indicating endothelial lineage) and the fibroblast marker FSP1 (also termed S100A4), a member of the S100 superfamily of EF-hand calcium-binding proteins. Cells expressing both β-gal and FSP1 were present in fibrotic hearts (**Fig. 1d**), whereas such double-positive cells were not detected in normal unbanded hearts (data not shown).

Next, we used *FSP1-GFP* mice, in which GFP is expressed under the control of the *FSP1* promoter[7], as a second genetic tool to investigate the occurrence of cardiac EndMT. After aortic banding, GFP staining was found within cardiac endothelial cells (marked by CD31 staining) in fibrotic hearts; coexpression of the fibroblast and endothelial cell markers suggests an early stage of EndMT (**Fig. 1e**). In control unbanded hearts, GFP expression was confined to sparsely scattered fibroblasts (**Fig. 1e**).

To gather further evidence for the acquisition of a mesenchymal phenotype by endothelial cells, we used fluorescence-activated cell sorting (FACS) to sort *lacZ*-positive cells (as assessed by staining for β-gal activity) from fibrotic banded and non-fibrotic non-banded *Tie1Cre;R26RstoplacZ* hearts. We used double labeling for *lacZ* and the endothelial marker CD31 to identify endothelial cells (*lacZ*$^+$CD31$^+$) and cells of endothelial origin that had lost expression of the endothelial marker (*lacZ*$^+$CD31$^-$). In normal hearts, *lacZ*$^+$CD31$^+$ cells represented the most prominent cell population (**Fig. 1f**). This cell population was considerably smaller in fibrotic hearts than in normal hearts, and the *lacZ*$^+$CD31$^-$ cell population was larger (**Fig. 1f**). We then compared *lacZ*$^+$CD31$^+$ and *lacZ*$^+$CD31$^-$ cells isolated from unbanded and banded fibrotic heart using real-time PCR. Expression of mRNAs corresponding to the mesenchymal markers α-SMA (smooth muscle actin), FSP1, the receptor tyrosine kinase DDR-2, and type I collagen α1 was substantially higher, and expression of the endothelial cell marker VE-cadherin was substantially lower, in the *lacZ*$^+$CD31$^-$ cell population compared to the *lacZ*$^+$CD31$^+$ cell population. The absence of CD31 expression in the *lacZ*$^+$CD31$^-$ population confirmed the purity of the sorted population (**Fig. 1g**).

Bone marrow–derived progenitor cells in cardiac fibrosis

Another possible source of fibroblasts in the stressed heart is bone marrow–derived progenitor cells. Recent studies have shown that

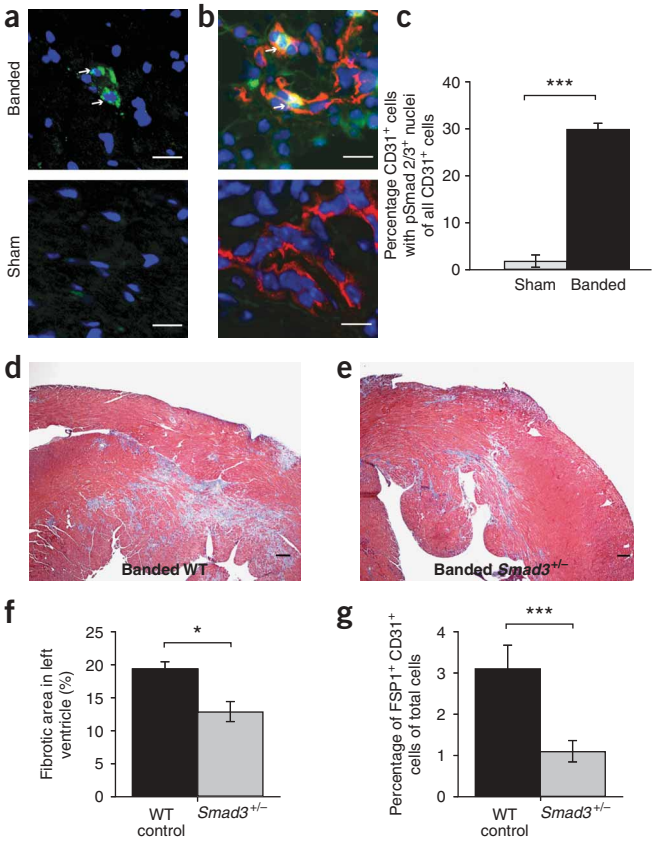

Figure 3 EndMT in cardiac fibrosis is mediated by TGF-β1 in a Smad-dependent manner. (**a**) In banded fibrotic hearts, TGF-β1 expression was detected by immunofluorescence (green; top, arrows), whereas no TGF-β1 staining was detected in sham-operated hearts (bottom). Scale bars, 20 μm. (**b**) Confocal microscopy of immunofluorescence double-labeling using antibodies specific to CD31 (red) and phosphorylated Smad2/3 (pSmad2/3; green) revealed nuclear pSmad2/3 staining in endothelial cells in banded hearts (arrows, top). No nuclear pSmad2/3 staining was found in endothelial cells from hearts of sham-operated mice (bottom). Nuclei were counterstained with TOPRO-3 (blue). Scale bars, 20 μm. (**c**) Percentages of $CD31^+pSmad2/3^+$ double-labeled cells in sham and banded hearts. $n = 6$ mice per group. (**d**–**g**) Aortic banding in *Smad3*$^{+/-}$ and wild-type mice. (**d**,**e**) Representative areas of Masson trichrome-stained banded hearts from a wild-type (WT) mouse (**d**) and a *Smad3*$^{+/-}$ mouse (**e**). Scale bars, 200 μm. (**f**) Morphometric analysis of cardiac fibrosis. (**g**) Quantification of cells positive for both FSP1 and CD31. For **f** and **g**, $n = 3$ mice per group. * $P \leq 0.05$, *** $P \leq 0.001$.

Tie1$^+$ bone marrow–derived progenitor cells exist in tissues[15]. Therefore, we addressed the possibility that β-gal$^+$ fibroblasts observed in banded hearts could be derivatives of such Tie1$^+$ progenitor cells. To test this notion, we transplanted irradiated C57BL/6 mice with *Tie1Cre;R26RstoplacZ* bone marrow (**Fig. 2a–c**), and carried out aortic banding 3 weeks later. About 12% of all bone marrow cells were *lacZ* positive (in both banded and unbanded mice) (**Fig. 2a**,**c**); this result is consistent with previous data, in which 14–20% of hematopoietic progenitor cells are *lacZ* positive in adult *Tie1Cre;R26RstoplacZ* mice[15], and indicates that the bone marrow was fully reconstituted by the transplanted cells. In the hearts of normal (unbanded) mice that received *Tie1Cre;R26RstoplacZ* bone marrow, 0.19% of all cells in the heart were *lacZ*$^+$. In the hearts of bone marrow–transplanted mice with fibrosis (banded), 1.2% of all cells in the heart were *lacZ*$^+$ (**Fig. 2b**,**c**). Such cells were detected exclusively in vessels, confirming previous studies in which Tie1$^+$ endothelial progenitors were shown to contribute to vascular regeneration (**Fig. 2b**)[18]. Although the number of *lacZ*$^+$ cells in banded hearts was low, our results indicate that these progenitor cells do not contribute to FSP1$^+$*lacZ*$^+$ or α-SMA$^+$*lacZ*$^+$ double-positive cells, as none of the *lacZ*$^+$ cells were positive for FSP1 or α-SMA (**Fig. 2b**). Therefore, Tie1$^+$ endothelial cells, but not Tie1$^+$ bone marrow–derived cells, contribute to the generation of fibroblasts in heart tissue.

To test whether bone marrow–derived cells can contribute to FSP1$^+$ or α-SMA$^+$ fibroblasts in banded hearts, we performed bone marrow transplantation of male wild-type C57BL/6 bone marrow into irradiated female wild-type C57BL/6 mice, followed by aortic banding (**Fig. 2d–g**). All bone marrow cells had a Y chromosome 3 weeks after transplantation, indicating that the female bone marrow had been completely reconstituted by the transplanted cells from the male donor (**Fig. 2d**). In the banded hearts, 25.7% of all cells carried a Y chromosome, indicating their bone marrow origin, whereas in normal hearts, only 3.9% of all cells were derived from the bone marrow (**Fig. 2e**). These results are consistent with a previous study that showed that in fibrotic areas of myocardial infarction about 25% of cells are derived from bone marrow, whereas in normal hearts about 4% of all cells are from the bone marrow[19]. In banded hearts, we detected a Y chromosome in 13.4% of FSP1$^+$ cells and in 21.1% of α-SMA$^+$ cells, indicating that these fibroblasts originate from bone marrow cells (**Fig. 2f**,**g**). In unbanded hearts, the number of FSP1-positive cells was very low (**Fig. 2e**,**f**), and we did not detect any FSP1-positive cells with a Y chromosome (**Fig. 2f**); in unbanded hearts, 3.4% of α-SMA$^+$ cells carried a Y chromosome (**Fig. 2g**). These results indicate that bone marrow cells can contribute to the population of cardiac fibroblasts, but not to those with an endothelial-cell imprint.

EndMT is mediated by TGF-β1

Next, we investigated the involvement of TGF-β1 signaling in banded hearts. Gene expression analysis has shown that the progression of fibrosis due to aortic banding is associated with increased expression of the mRNA encoding TGF-β1 (O.T., W.P and S.I., unpublished results available at http://www.cardiogenomics.org). Inhibition of myocardial fibrosis by blocking TGF-β function has been previously described in the pressure-overload rat model[20]. We further confirmed the involvement of TGF-β1 signaling by immunofluorescence labeling of hearts from banded mice and sham-operated control mice (**Fig. 3a**). Smad2 and Smad3 (Smad2/3) are the major mediators of TGF-β1 signaling in endothelial cells[21]. Nuclear staining of phosphorylated Smad2/3 was present in 30% of endothelial cells of banded hearts, compared to less than 2% of endothelial cells in sham-operated hearts (**Fig. 3b**,**c**), illustrating active TGF-β1 signaling in the endothelial cells of banded hearts. This result suggests that EndMT might be mediated by TGF-β1 in a Smad-dependent manner.

Homozygous deletion of TGF-β1 or Smad3 results in death at an early age[22–24]. To assess the contribution of TGF-β1 signaling in EndMT and cardiac fibrosis, we therefore performed experiments using *Smad3*$^{+/-}$ mice. In these mice, *Smad3* mRNA levels are reduced by approximately 50%, and wound healing and inflammation are reduced[22–24]. In our experiments, progression of cardiac fibrosis was significantly inhibited in *Smad3*$^{+/-}$ mice (**Figs. 3d–f**). The decrease in cardiac fibrosis was associated with a significant decrease in the number of CD31$^+$FSP1$^+$ cells (**Fig. 3g**), indicating that TGF-β1 signaling contributes to EndMT.

rhBMP-7 inhibits TGF-β1–induced EndMT *in vitro*

TGF-β, a mediator of EndMT during the formation of the atrioventricular canal[8], also promotes cardiac fibrosis[25,26]. Incubation of adult human coronary endothelial cells (HCEC) with TGF-β1 resulted in a fibroblast-like phenotype (**Fig. 4a**), similar to the phenotypic changes associated with EndMT as observed in experiments using explants of the atrioventricular cushion (**Supplementary Fig. 1** online). In spindle-shaped TGF-β1–treated HCEC, the expression of proteins associated with fibroblasts (FSP1, vimentin, pro-collagen I and α-SMA) was upregulated, whereas the expression of proteins associated with endothelial cells (CD31 and VE-cadherin) was downregulated (**Supplementary Fig. 2** online).

BMP-7 is a member of the TGF-β superfamily of growth factors[27]. BMPs in general are associated with morphogenesis in a variety of organs[27]. During cardiac development, BMPs modulate the formation of the atrioventricular cushion[10]. The specific role of BMP-7 on this EndMT in cardiac development is unclear. We tested the effect of BMP-7 on TGF-β1–induced EndMT in HCEC by exposing HCEC to various concentrations of rhBMP-7 (0.1–10,000 ng/ml) and TGF-β1. Although incubation with rhBMP-7 alone had no obvious effect on the phenotype of HCEC, rhBMP-7 substantially inhibited TGF-β–induced EndMT at an optimal concentration of 1,000 ng/ml (**Fig. 4a**,**b**). We also assessed the effect of TGF-β1 and rhBMP-7 on type I collagen and fibronectin expression in HCEC. Both type I collagen and fibronectin were expressed at higher levels in tissue culture supernatants of TGF-β1–treated HCEC than in supernatants from untreated control cells (**Fig. 4c**,**d**). These TGF-β1–mediated effects were significantly inhibited by rhBMP-7 (**Fig. 4c**,**d**). Cell viability was reduced by treatment with TGF-β1 (**Fig. 4e**). In control experiments, rhBMP-7 had a negligible effect on the proliferation of primary cardiac fibroblasts (**Supplementary Fig. 3** online).

rhBMP-7 reduces fibrosis in pressure overloaded mice

In the pressure overload mouse model, constriction (by banding) of the ascending aorta causes cardiac hypertrophy 48 h after surgery and leads to fibrosis 5 d after surgery[28]. We administered rhBMP-7 (300 μg per kilogram body weight every other day) starting 1 d before surgery and lasting until the end of the study (28 d) using FVB/N mice. Analysis of Masson's trichrome-stained sections of hearts from mice that had received rhBMP-7 showed a significant reduction of fibrosis within the left ventricle by about 40% as compared to vehicle-treated banded mice (**Fig. 5a**,**b**). Aortic banding resulted in increased deposition of collagens type I and III and accumulation of vimentin-positive cells, as well as rarification of the microvasculature (indicated by reduced CD31 staining). Administration of rhBMP-7 reduced the accumulation of ECM and fibroblasts and resulted in an increased microvascular density compared with vehicle-administered controls (**Supplementary Fig. 4** online).

The pressure overload model is commonly associated with fibrotic lesions and diastolic dysfunction (as assessed by the left-ventricular end-diastolic pressure (LVEDP), the maximum rate of left ventricular pressure decline $(dp/dt)_{min}$, the relaxation constant τ_{Glantz}, and the end-diastolic pressure-volume relationship (EDPVR))[29,30]. In the current study we examined LVEDP and $(dp/dt)_{min}$. These hemodynamic data, together with the presence of fibrosis, indicate that our model of pressure overload was associated with diastolic dysfunction. Sham-operated mice had a LVEDP of 5 mm Hg, which was significantly elevated in vehicle-treated banded mice (15 mm Hg; **Fig. 5b**). LVEDP in rhBMP-7–administered banded mice was reduced to 11 mm Hg (**Fig. 5b**). Furthermore, $(dp/dt)_{min}$ was greater in rhBMP-7–treated banded mice (–8,922 ± 752 mm Hg/s) than in vehicle-treated banded mice (–7,514 ± 169 mm Hg/s, $P = 0.058$). Taken together, these results indicate that a reduction in fibrosis by rhBMP-7 was associated with improved diastolic cardiac function. Although both vehicle- and rhBMP-7–treated banded mice had a significantly elevated left ventricular systolic pressure (LVSP) when compared to sham-operated mice (75 ± 2 mm Hg), the LVSP was similar between vehicle-treated banded mice (157 ± 6 mm Hg) and rhBMP-7–treated banded mice (152 ± 11 mm Hg). Systolic function was normal in all groups, as measured by fractional shortening during echocardiography (**Fig. 5b** and **Supplementary Table 1**

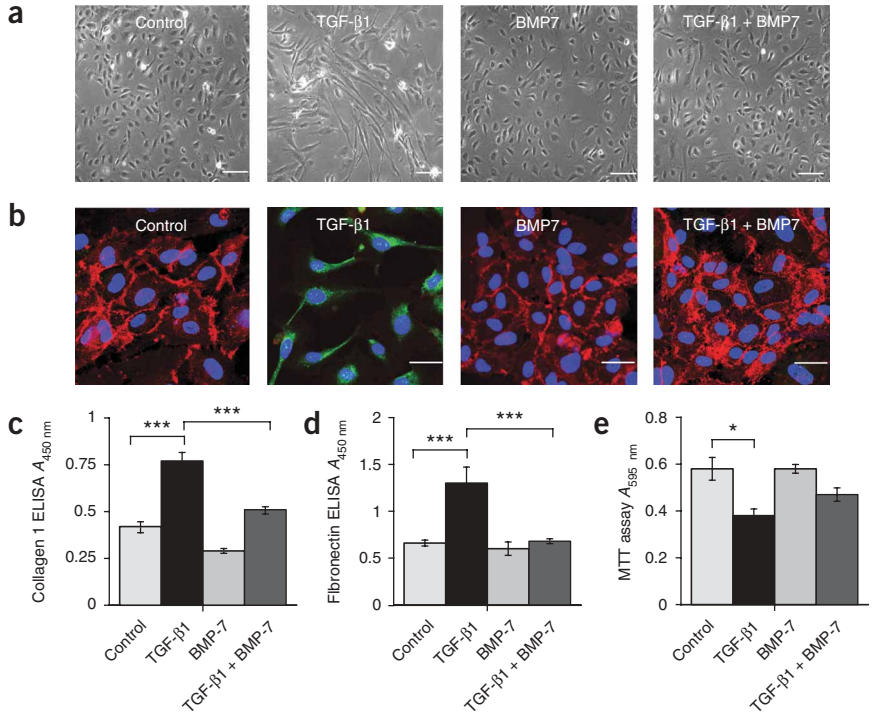

Figure 4 rhBMP-7 inhibits TGF-β1–induced EndMT in HCEC. HCEC were treated with TGF-β1, rhBMP-7, or TGF-β1 + rhBMP-7, or cultured as untreated controls for 6 d. (**a**) Representative bright-field images of each group. TGF-β1-treated HCEC had a fibroblast-like phenotype, whereas untreated control cells and rhBMP-7–treated cells preserved their endothelial cell phenotype. rhBMP-7 blocked the effect of TGF-β1 treatment and the morphology of the cells was similar to that of untreated control cells. Scale bars, 25 μm. (**b**) Representative confocal images of CD31 (red) and FSP1 (green) staining in each group. Nuclei were counterstained with TOPRO-3 (blue). Acquisition of a spindle-shaped morphology upon TGF-β1 exposure correlated with FSP1 staining and loss of CD31 staining. Co-incubation with rhBMP-7 neutralized the TGF-β1–induced phenotypic change. Scale bars, 20 μm. (**c**–**e**) Quantification of collagen type I (**c**) and fibronectin (**d**) ELISAs from the supernatants of the different cell groups. (**e**) Cell viability was assessed with the MTT assay. Experiments were repeated three times. * $P \leq 0.05$, *** $P \leq 0.001$.

online). The left ventricular wall thickness was significantly increased in banded mice compared with sham-operated mice, but was unchanged in rhBMP-7–treated compared with vehicle-treated banded mice, indicating that rhBMP-7 affects fibrosis but not hypertrophy (**Supplementary Table 1**). Consistent with this concept, cardiomyocytes in banded hearts were significantly larger than those in the hearts of sham-operated mice, as assessed using H&E-stained sections (**Supplementary Fig. 4** online). No difference in the size of cardiomyocytes was seen between rhBMP-7–treated and vehicle-treated banded mice.

Inhibition of fibrosis correlates with reduction of EndMT

By performing double labeling experiments using antibodies to α-SMA and FSP1, we established that FSP1 and α-SMA mark different subpopulations of fibroblasts with a small overlap of the two markers, confirming previous studies of tumor fibrosis[31]. We evaluated the effect of rhBMP-7 administration on EndMT in banded hearts with fibrosis from *Tie1Cre;R26RstoplacZ* mice. In these hearts, 14% of FSP1$^+$ fibroblasts were *lacZ*$^+$, whereas 75% of α-SMA$^+$ fibroblasts were *lacZ*$^+$ (**Fig. 5c–f**). Based on these results, we estimate that 27–35% of all fibroblasts (either FSP1$^+$ or α-SMA$^+$) are of endothelial origin (**Supplementary Fig. 5** and **Supplementary Note** online). In rhBMP-7–treated mice, the number of EndMT-derived fibroblasts was significantly reduced (80% reduction for FSP1$^+$*lacZ*$^+$ fibroblasts and 66% reduction for α-SMA$^+$*lacZ*$^+$ cells; **Fig. 5c–f**). Analysis of FSP1/CD31 and α-SMA/CD31 double labeling revealed that cardiac fibrosis was associated with the presence of both FSP1$^+$CD31$^+$ and α-SMA$^+$CD31$^+$ double-positive cells, and rhBMP-7 administration greatly reduced the number of such double-positive cells (**Fig. 5g**). The percentage of FSP1-positive cells of all heart cells was also significantly decreased in rhBMP-7–treated mice (**Fig. 5e**), possibly reflecting a reduction in the number of EndMT-derived fibroblasts. Administration of rhBMP-7 also decreased the percentage of α-SMA$^+$ cells of all heart cells (**Fig. 5f**); however, in the banded heart this reduction was not statistically significant.

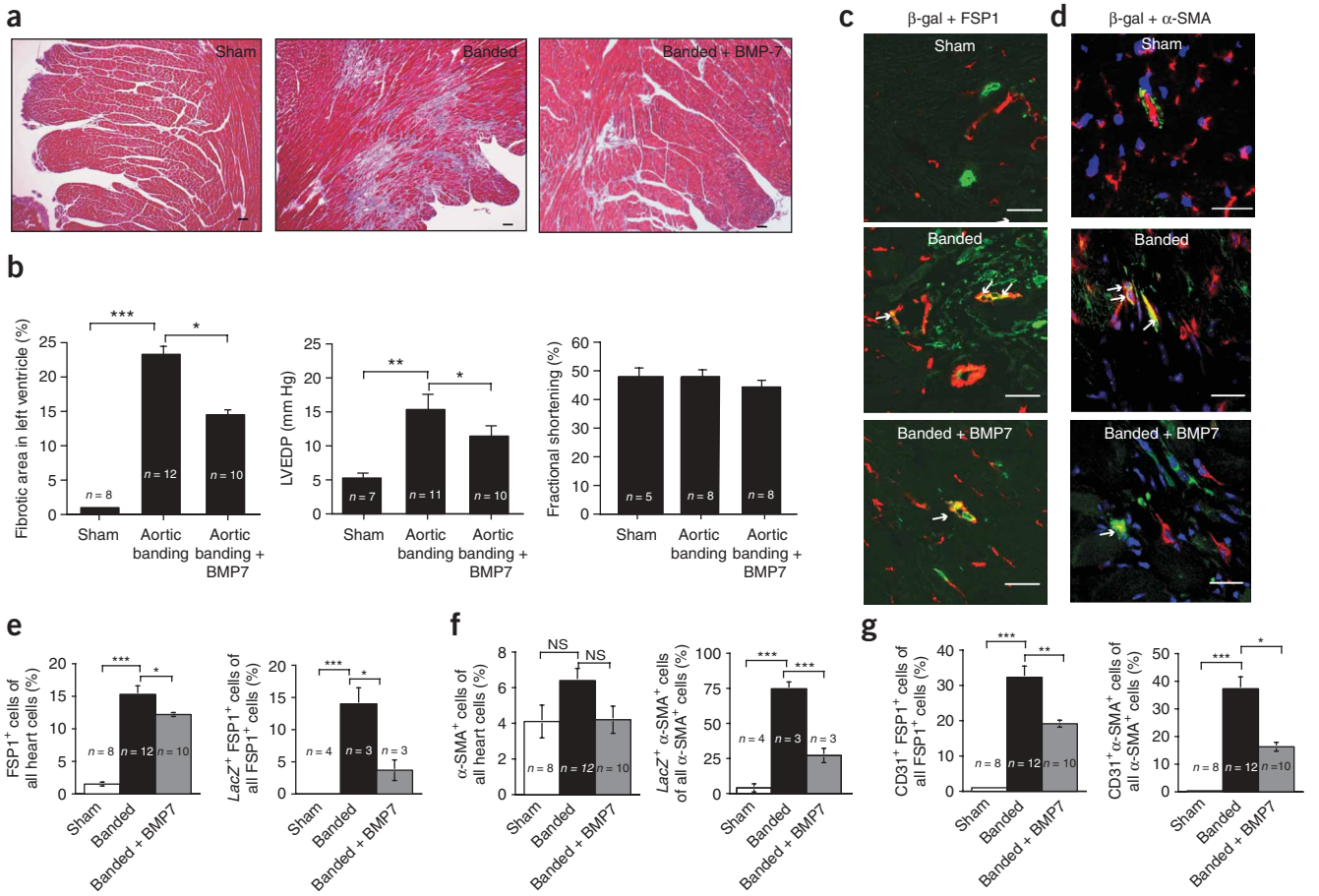

Figure 5 Inhibition of cardiac fibrosis induced by aortic banding by rhBMP-7 is associated with inhibition of EndMT. Tissues were analyzed 4 weeks after banding. (**a**) Representative areas of Masson trichrome-stained hearts (fibrotic areas are stained blue) of sham, banded vehicle-treated and banded rhBMP-7–treated mice. Scale bars, 100 μm. (**b**) Quantification of the average fibrotic area, LVEDP and fractional shortening. (**c–g**) Tissue sections of sham-operated (top), banded vehicle-treated (middle) and banded rhBMP-7–treated (bottom) hearts were stained with antibodies to FSP1 (green, **c**) or α-SMA (green, **d**) and β-gal (red, **c**,**d**) to detect cells undergoing EndMT. (**c**) Double labeling for FSP1 and β-gal (**c**) or for α-SMA and β-gal (**d**) in *Tie1Cre;R26RstoplacZ* mice to detect FSP1-positive or α-SMA-positive fibroblasts of endothelial origin, respectively. No double-positive cells were present in the normal heart. Double-positive cells (arrows) were found in fibrotic areas of banded vehicle-treated hearts; fewer were found in banded hearts of rhBMP-7–treated mice. Nuclei were counterstained with TOPRO-3 (blue). Scale bars, 20 μm. (**e**) Percentage of cells that were FSP1$^+$ (left) and percentage of FSP1$^+$ cells that were FSP1$^+$*lacZ*$^+$ (right) for each group. (**f**) Percentage of cells that were α-SMA$^+$ (left) and percentage of α-SMA$^+$ cells that were α-SMA$^+$*lacZ*$^+$ for each group. (**g**) Tissue sections were labeled with antibodies to CD31 and FSP1 or α-SMA. The bar graphs depict the percentage of FSP1$^+$ cells that were CD31$^+$FSP1$^+$ (left) and the percentage of α-SMA$^+$ cells that were CD31$^+$α-SMA$^+$ (right) for each group. The number of hearts analyzed is indicated in the bar graphs. * $P \leq 0.05$; ** $P \leq 0.01$; *** $P \leq 0.001$; NS, not significant.

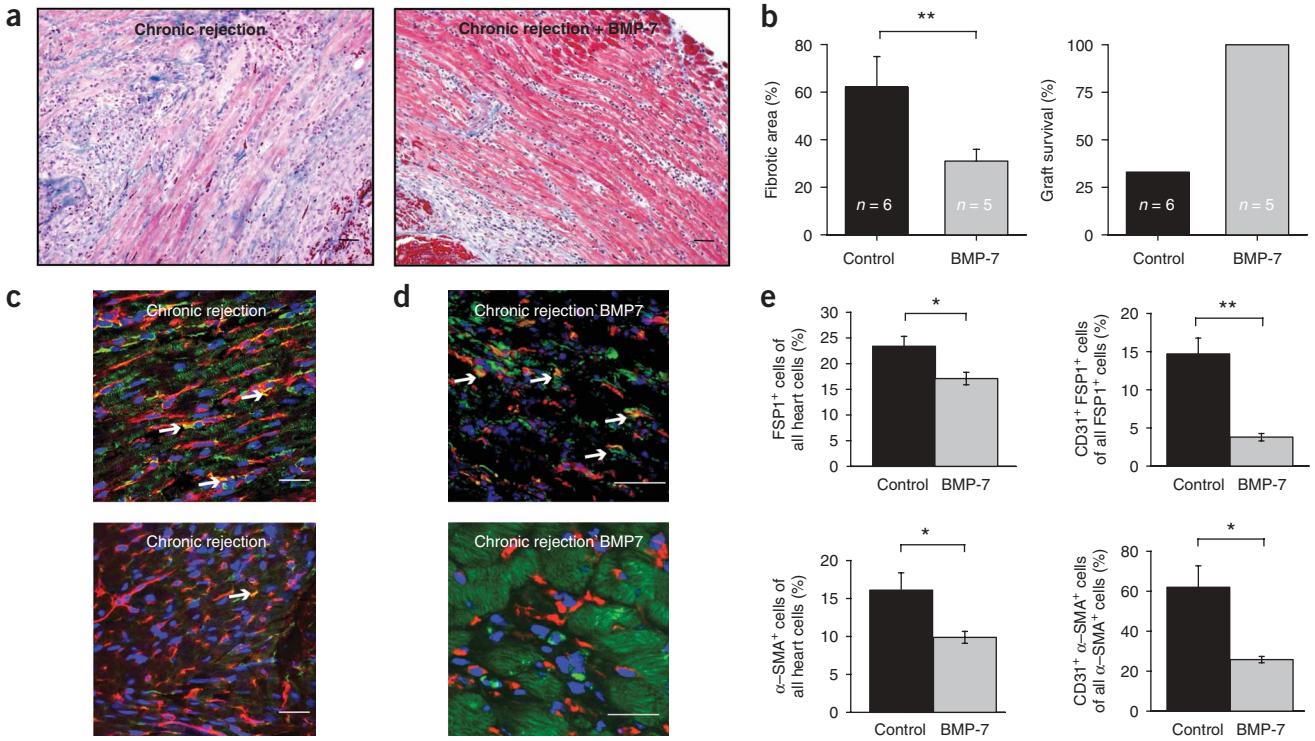

Figure 6 Treatment with rhBMP-7 inhibits cardiac fibrosis and reduces EndMT in a model of chronic rejection. Cardiac fibrosis was induced by heterotopic heart transplantation with a class II major histocompatibility difference between the donor and the recipient. Tissues were analyzed 8 weeks after surgery. (**a**) Representative areas of Masson trichrome-stained hearts of rhBMP-7–treated and vehicle-treated transplanted mice. Scale bars, 200 μm. (**b**) Left, average fibrotic area. Right, graft survival, assessed by palpation of the abdominal cavity. The number of hearts analyzed is indicated in the bar graphs. (**c**,**d**) Tissue sections of vehicle-treated (chronic rejection) and rhBMP-7–treated (chronic rejection + BMP-7) transplanted hearts were stained with antibodies to FSP1 (green, **c**) or α-SMA (green, **d**) and CD31 (red, **c**,**d**). FSP1$^+$CD31$^+$ (**c**) and α-SMA$^+$CD31$^+$ (**d**) cells (arrows) were abundant in vehicle-treated hearts (**c**,**d**, top micrographs), but were rare in rhBMP-7–treated hearts (**c**,**d**, bottom micrographs). Scale bars, 25 μm. (**e**) Percentage of heart cells that were positive for FSP1 (top left) and α-SMA (bottom left), and the percentage of cells undergoing EndMT, as assessed by FSP1/CD31 (top right) or α-SMA/CD31 (bottom right) double labeling. $n = 6$ vehicle-treated (control) and 5 BMP-7-treated hearts. $^*P \leq 0.05$, $^{**}P \leq 0.01$.

rhBMP-7 reduces fibrosis in chronic rejection

We next tested the effect of rhBMP-7 administration on cardiac fibrosis and EndMT in a mouse model of chronic heart rejection. In this model, heterotopic heart transplantation with a class II major histocompatibility difference between the donor and the recipient leads to fibrosis[32]. As with banded hearts, we evaluated cardiac fibrosis in transplanted hearts by Masson's trichrome labeling. Fibrosis was reduced by 50% in rhBMP-7–treated mice compared to vehicle-treated mice (**Fig. 6a**,**b**).

Graft survival in this model is assessed by palpation of the heartbeat in the abdomen. Four of six hearts stopped beating in vehicle-treated mice before the end of the study, but all hearts in the rhBMP-7 treated group were still beating after 56 d (**Fig. 6b**), indicating that decreased fibrosis was associated with functional improvement. Chronic rejection in this model results in an accumulation of vimentin-positive cells, increased deposition of collagen I and III, and rarification of the microvasculature (as indicated by reduced CD31 staining). Administration of rhBMP-7 reduced the accumulation of ECM and fibroblasts and preserved the microvasculature (**Supplementary Fig. 4**). Cardiac fibrosis in this model was associated with the presence of both FSP1$^+$CD31$^+$ and α-SMA$^+$CD31$^+$ double-positive cells, as assessed by double labeling experiments (**Fig. 6c**). Administration of rhBMP-7 markedly reduced the number of such double-positive cells (**Fig. 6d**,**e**). The percentages of FSP1-positive and α-SMA-positive cells of all heart cells were also significantly decreased in rhBMP-7–treated mice (**Fig. 6e**).

BMP-7 acts through three possible receptors—activin-like kinase receptor (ALK) 2, ALK3 and ALK6; these function in combination with the BMP receptor BMPR-II. Real-time PCR analysis of cardiac endothelial cells (*lacZ*$^+$CD31$^+$) and cells of endothelial origin with an acquired mesenchymal phenotype (*lacZ*$^+$CD31$^-$; see populations R4 and R6, respectively, in **Fig. 1f**) showed that mRNAs corresponding to BMP-7 and ALK6 were not detected in either cell population; however, mRNAs corresponding to the BMP-7 receptors ALK2, ALK3 and BMPR-II were present in both populations (**Supplementary Fig. 6** online). BMP-7 signaling is mediated by Smad1, and in the hearts of mice administered rhBMP-7, nuclear staining for phosphorylated Smad1 was detected in 69% of endothelial cells compared to 11% in untreated hearts (**Supplementary Fig. 6**). These results indicate that BMP-7 signaling is activated in the endothelial cells of rhBMP-7 administered mice.

Finally, to confirm the therapeutic specificity of rhBMP-7–mediated effects in the heart, we performed experiments using neutralizing antibodies specific to BMP-7, recombinant noggin (a physiological inhibitor of BMP-7, which acts by binding BMP-7 extracellularly), and a soluble Alk3-Fc chimera protein (which acts as an extracellular trap for various BMPs including BMP-7). All three BMP-7 inhibitors reversed the effects of rhBMP-7 on TGF-β1–induced EndMT (**Supplementary Fig. 6**). In addition, when banded mice with cardiac fibrosis were treated with BMP-7-neutralizing antibodies in combination with rhBMP-7 (administered on alternate days), the therapeutic effect of rhBMP-7 was abolished (**Supplementary Fig. 6**).

DISCUSSION

Cardiac fibrosis is a common feature in patients with advanced cardiac failure, regardless of the etiology of cardiomyopathy. It is recognized that anti-fibrotic therapies might be useful in improving cardiac function of the diseased heart. However, the development of such therapies has been limited by an incomplete understanding of the origin of fibroblasts in the heart. Here we show that cardiac fibrosis is associated with the emergence of fibroblasts with an endothelial cell origin. Our experiments show that TGF-β1–induced EndMT in adult human coronary endothelial cells can be inhibited by rhBMP-7 and that systemic administration of rhBMP-7 ameliorates the progression of cardiac fibrosis in two independent mouse models of heart disease. These studies do not exclude the possibility that other BMPs could elicit similar anti-fibrotic effects in the heart, and this notion needs further testing. Our results, which suggest that rhBMP-7 protects the heart by inhibiting TGF-β1–induced EndMT, are consistent with a study showing that, in a mouse model of ischemic injury, rhBMP-7 injected into the heart stabilizes the microvasculature[33]. We cannot exclude the possibility that rhBMP-7, in addition to inhibiting EndMT, might also elicit anti-inflammatory effects, promote myogenesis or prevent apoptosis of endothelial cells[34]. The precise triggers of TGF-β expression in fibrotic hearts are unknown, but it has been proposed that hemodynamic stress could trigger a pro-inflammatory process in the vicinity of the intracardiac vasculature, leading to the activation of endothelial cells; these cells in turn can produce fibrogenic mediators and induce fibroblast activation and myocardial fibrosis[35–38]. On the basis of our findings, we speculate that TGF-β not only activates endothelial cells to produce fibrogenic mediators, but also induces EndMT. Our study provides evidence that the inhibition of EndMT by rhBMP-7 may be a viable therapeutic strategy against cardiac fibrosis.

METHODS

Materials. For *in vivo* studies, we used an rhBMP-7 homodimer, non-covalently attached to a prodomain protein (referred to as soluble rhBMP-7)[39]. In cell culture experiments, we used active rhBMP-7 (ref. 39). rhBMP-7 (both soluble and active) was provided as a research gift by Curis, Inc.

Mice. The *Tie1Cre* and *R26RstoplacZ* alleles have been described[17,19]. Transgenic mice that express GFP under the control of the FSP1 promoter and mice carrying a mutant *Smad3* allele have been described[7,36]. All procedures were carried out with the approval of the Institutional Animal Care and Use Committee of the Beth Israel Deaconess Medical Center.

Culture of human coronary endothelial cells (HCEC). HCEC were used between the third and fifth passage. Cells were treated with 10 ng/ml TGF-β1; 1,000 ng/ml rhBMP-7; 10 ng/ml TGF-β1 plus 1,000 ng/ml rhBMP-7; or control medium without growth factors, for 1 week. In control experiments, BMP-7-neutralizing antibodies (Curis, 13.65 μg/ml), soluble Alk3-Fc chimera (R&D Systems, 10 μg/ml) or recombinant mouse noggin (R&D Systems, 1 μg/ml) were added to the medium. HCEC were a gift from W.C. Aird (Beth Israel Deaconess Medical Center, Boston).

Generation of mice with aortic constriction. Ascending aortic constriction was performed in 12-week-old male FVB/N mice as described[40]. rhBMP-7 was administered intraperitoneally every other day, starting 1 d before surgery, for the 4-week duration of the study. After 1 week, echocardiography was performed, and both echocardiography and invasive hemodynamics were performed before mice were killed. Ascending aortic constriction was also performed on 16-week-old *Smad3*$^{+/-}$ male mice and wild-type male littermates or 24-week-old *Tie1Cre;R26RstoplacZ* male mice and wild-type male littermates, all on a C57BL/6 background. For aortic constriction in bone marrow transplanted mice, 24-week-old female wild-type C57BL/6 mice were used. All mice used weighed 25–30 g. For sham-operated animals, the chest was surgically opened under the same conditions as banded mice, except that no aortic banding was performed. The term 'unbanded hearts' refers to normal hearts obtained from mice without a sham operation.

Hemodynamic measurement. At day 28, hemodynamic measurements were performed as described, using the open-chest technique[39].

Generation of mice with chronic rejection. Heterotopic heart transplantation was performed into the abdomen of the recipient mouse, with a class II major histocompatibility difference between donor and recipient (BM12 into B6)[30]. Recipient mice were subjected to chronic allograft rejection for 56 d. rhBMP-7–treated mice received rhBMP-7 every other day, starting 1 d before surgery, for the 8-week duration of the study.

Bone marrow transplantation experiments. Bone marrow transplantation was performed as described[41,42]. Bone marrow cells were taken from *Tie1Cre;R26RstoplacZ* double transgenic or male wild-type C57BL/6 donor mice. Aortic banding was performed 3 weeks after bone marrow transplantation and mice were killed 1 week after aortic banding.

Histological assessment of cardiac fibrosis. The percent area of myocardial fibrosis was calculated as described[39,43]. In banded mice, only fibrosis in the left ventricle was evaluated; in transplanted mice, both ventricles were analyzed. Cardiomyocyte size determination was performed as described[44].

Immunofluorescence. We performed immunofluorescence staining as described[45]. In fibrotic hearts, evaluation was performed within fibrotic regions. Only tissue within 300 μm of fibrotic tissue was analyzed.

***LacZ* staining.** Frozen tissue was cut into 5 μm thick cross-sections which were fixed in 4% PFA at 4 °C for 10 min. Sections were washed 3 times in PBS and then incubated at 37 °C in 1 mg/ml X-gal (Sigma), 5 mM potassium ferrocyanide, 5 mM potassium ferricyanide, 2 mM $MgCl_2$, 0.2% NP-40 and 0.1% Na-deoxycholate in PBS for 72 h[46].

Fluorescence *in situ* hybridization. We performed fluorescence *in situ* hybridization (FISH) using the Starfish Y chromosome labeling kit (Open Biosystems) according to the manufacturer's instructions. For combined FISH and immunohistochemistry, we first performed immunohistochemistry, followed by the FISH protocol. In two male control hearts (positive control), 60% of cardiomyocyte nuclei and 67% of other cells contained a detectable Y chromosome. This incomplete detection reflects the fact that, in a 5 μm-thick section, the Y chromosome in any particular cell may not be included in the section. The percentage of cells with a Y chromosome detected in the hearts of bone marrow–transplanted mice was not divided by a correction factor. No Y chromosomes were detected in two female control hearts (negative control).

Direct ELISA. We performed ELISAs for estimation of type I collagen and fibronectin as described, with minor modifications[39]. HCEC cells (8×10^3 cells per well in 96-well plates) were stimulated with growth factors in basal-medium 2 (Clonetics) supplemented with 50 μg/ml ascorbic acid and aminopropionitrile (Sigma) for 48 h.

MTT assay. HCEC cells (5,000 cells per well) were plated in a 96-well plate in basal medium-2 (Clonetics). The next day, growth factors were added according to the experimental protocol. Cell viability was evaluated after 7 d as described[47].

FACS sorting. Single cells were isolated from hearts of banded and normal *Tie1Cre;R26RstoplacZ* mice according to a method that was previously described for sorting of mouse cardiac endothelial cells[48]. We used the *In vivo* LacZ β-Galactosidase Detection Kit (Marker Gene Technologies) according to the manufacturer's recommendations. As a positive control for *lacZ* staining, isolated cells from the heart of a *Rosa26* mouse with ubiquitous *lacZ* expression were used. For CD31 labeling, a PE-conjugated antibody specific to CD31 was used (Pharmingen), following the *lacZ* staining. Flow cytometric analysis and sorting of *lacZ*$^+$CD31$^+$ or *lacZ*$^+$CD31$^-$ cells using a high-speed cell sorter (MoFlo-MLS, Cytomation) were performed as described[49].

RNA isolation and quantitative real-time PCR. One thousand *lacZ*$^+$CD31$^+$ or *lacZ*$^+$CD31$^-$ cells were directly collected into lysis buffer and RNA was isolated according to the manufacturer's instruction (Cells-to-cDNA II Kit, Ambion). Specific primers (**Supplementary Table 2** online) were designed using the Primer Express 1.5 program. 18S rRNA (Pre-Developed TaqMan Assay Reagents, Applied Biosystems) was used as an internal standard. RT-PCR was carried out in a 7000 Sequence Detector System (Applied Biosystems), and measurements were standardized to the 18S rRNA reaction using standard calculation methods as described[50].

Statistical analysis. Data are presented as mean ± s.e.m. We used ANOVA with subsequent Bonferroni or Dunnett's test to determine the significance in multiple comparisons. We used the Mann-Whitney *U*-test to compare the mean of two groups. Values of $P < 0.05$ were considered statistically significant.

Note: Supplementary information is available on the Nature Medicine website.

ACKNOWLEDGMENTS
This study was partially funded by research grants DK62987, AA13913, DK61688 and DK55001 from the NIH, partially by a research grant from Novartis Corporation, and partly by a research fund from the Beth Israel Deaconess Medical Center for the Division of Matrix Biology. E.Z. was funded by a fellowship grant from the Leopoldina Academy (BMBF-LPD 9901/8-105) and is currently funded by a Ruth L. Kirschstein National Research Service Award from the NIH (5 F32 HL082436-01). M.Z. is funded by NIH grant 5K08DK074558-01 and the ASN Carl W. Gottschalk Award. EGN is funded by a NIH grant (DK-46282). Parts of this study were presented as an oral presentation at the American Heart Association 2004. We thank V. Toxavidis and J. Tigges from the Beth Israel Deaconess Medical Center Flow Cytometry and Cell Sorting Core Facility for their help with the FACS sorting as well as S. McGoohan for technical assistance with the real-time PCR.

AUTHOR CONTRIBUTIONS
E.M.Z.: tissue analysis, immuno-labeling, FISH, EndMT cell culture experiments, bone marrow transplantation, animal husbandry, design of experiments, data analysis and interpretation, substantial contribution to manuscript preparation, writing and generation of all figures. O.T.: All aortic banding surgeries and invasive hemodynamic measurements. M.Z.: isolation of primary heart fibroblasts, MTT assay, collagen ELISA, contribution to conceptual design, data analysis, data discussion and manuscript editing. A.L.D.: echocardiography of mice. J.R.M.: data discussion and manuscript editing. E.G.: generation of Tie1Cre mice. A.C.: study design of transplantation experiments. X.Y.: transplantation surgeries. W.T.P.: AV cushion isolation. A.B.R.: generation of *Smad3*$^{+/-}$ mice. E.G.N.: manuscript editing, data discussion, generation of FSP1-GFP mice. M.H.S.: study design of transplantation experiments. S.I.: contribution to conceptual design of aortic banding experiments, manuscript editing, data discussion. R.K.: principal investigator of the study; overall study design to address the conceptual ideas; analysis and interpretation of the data, drafting and final editing of the manuscript.

COMPETING INTERESTS STATEMENT
The authors declare no competing financial interests.

Published online at http://www.nature.com/naturemedicine
Reprints and permissions information is available online at http://npg.nature.com/reprintsandpermissions

1. Jalil, J.E. *et al.* Fibrillar collagen and myocardial stiffness in the intact hypertrophied rat left ventricle. *Circ. Res.* **64**, 1041–1050 (1989).
2. Kass, D.A., Bronzwaer, J.G. & Paulus, W.J. What mechanisms underlie diastolic dysfunction in heart failure? *Circ. Res.* **94**, 1533–1542 (2004).
3. Vasan, R.S. & Benjamin, E.J. Diastolic heart failure—no time to relax. *N. Engl. J. Med.* **344**, 56–59 (2001).
4. Weber, K.T. Monitoring tissue repair and fibrosis from a distance. *Circulation* **96**, 2488–2492 (1997).
5. Maric, C., Ryan, G.B. & Alcorn, D. Embryonic and postnatal development of the rat renal interstitium. *Anat. Embryol. (Berl.)* **195**, 503–514 (1997).
6. Lang, H. & Fekete, D.M. Lineage analysis in the chicken inner ear shows differences in clonal dispersion for epithelial, neuronal, and mesenchymal cells. *Dev. Biol.* **234**, 120–137 (2001).
7. Iwano, M. *et al.* Evidence that fibroblasts derive from epithelium during tissue fibrosis. *J. Clin. Invest.* **110**, 341–350 (2002).
8. Eisenberg, L.M. & Markwald, R.R. Molecular regulation of atrioventricular valvuloseptal morphogenesis. *Circ. Res.* **77**, 1–6 (1995).
9. Liebner, S. *et al.* Beta-catenin is required for endothelial-mesenchymal transformation during heart cushion development in the mouse. *J. Cell Biol.* **166**, 359–367 (2004).
10. Nakajima, Y., Yamagishi, T., Hokari, S. & Nakamura, H. Mechanisms involved in valvuloseptal endocardial cushion formation in early cardiogenesis: roles of transforming growth factor (TGF)-beta and bone morphogenetic protein (BMP). *Anat. Rec.* **258**, 119–127 (2000).
11. Boyer, A.S. *et al.* TGFβ2 and TGFβ3 have separate and sequential activities during epithelial-mesenchymal cell transformation in the embryonic heart. *Dev. Biol.* **208**, 530–545 (1999).
12. Camenisch, T.D. *et al.* Temporal and distinct TGFβ ligand requirements during mouse and avian endocardial cushion morphogenesis. *Dev. Biol.* **248**, 170–181 (2002).
13. Lijnen, P.J., Petrov, V.V. & Fagard, R.H. Induction of cardiac fibrosis by transforming growth factor-β_1. *Mol. Genet. Metab.* **71**, 418–435 (2000).
14. Ramsdell, A.F. *et al.* Identification of an autocrine signaling pathway that amplifies induction of endocardial cushion tissue in the avian heart. *Acta Anat.* **162**, 1–15 (1998).
15. Gustafsson, E., Brakebusch, C., Hietanen, K. & Fassler, R. Tie-1-directed expression of Cre recombinase in endothelial cells of embryoid bodies and transgenic mice. *J. Cell Sci.* **114**, 671–676 (2001).
16. Mao, X., Fujiwara, Y. & Orkin, S.H. Improved reporter strain for monitoring Cre recombinase-mediated DNA excisions in mice. *Proc. Natl. Acad. Sci. USA* **96**, 5037–5042 (1999).
17. Korhonen, J., Polvi, A., Partanen, J. & Alitalo, K. The mouse tie receptor tyrosine kinase gene: expression during embryonic angiogenesis. *Oncogene* **9**, 395–403 (1994).
18. Rafii, S. & Lyden, D. Therapeutic stem and progenitor cell transplantation for organ vascularization and regeneration. *Nat. Med.* **9**, 702–712 (2003).
19. Hocht-Zeisberg, E. *et al.* Cellular repopulation of myocardial infarction in patients with sex-mismatched heart transplantation. *Eur. Heart J.* **25**, 749–758 (2004).
20. Kuwahara, F. *et al.* Transforming growth factor-beta function blocking prevents myocardial fibrosis and diastolic dysfunction in pressure-overloaded rats. *Circulation* **106**, 130–135 (2002).
21. Lebrin, F. *et al.* TGF-beta receptor function in the endothelium. *Cardiovasc. Res.* **65**, 599–608 (2005).
22. Yang, X. *et al.* Targeted disruption of SMAD3 results in impaired mucosal immunity and diminished T cell responsiveness to TGF-beta. *EMBO J.* **18**, 1280–1291 (1999).
23. Ashcroft, G.S. *et al.* Mice lacking Smad3 show accelerated wound healing and an impaired local inflammatory response. *Nat. Cell Biol.* **1**, 260–266 (1999).
24. Tokumasa, A. *et al.* Reduction of Smad3 accelerates re-epithelialization in a murine model of colitis. *Biochem. Biophys. Res. Commun.* **317**, 377–383 (2004).
25. Potts, J.D. & Runyan, R.B. Epithelial-mesenchymal cell transformation in the embryonic heart can be mediated, in part, by transforming growth factor beta. *Dev. Biol.* **134**, 392–401 (1989).
26. Verheule, S. *et al.* Increased vulnerability to atrial fibrillation in transgenic mice with selective atrial fibrosis caused by overexpression of TGF-beta1. *Circ. Res.* **94**, 1458–1465 (2004).
27. Hogan, B.L. Bone morphogenetic proteins in development. *Curr. Opin. Genet. Dev.* **6**, 432–438 (1996).
28. Tarnavski, O. *et al.* Mouse cardiac surgery: comprehensive techniques for the generation of mouse models of human diseases and their application for genomic studies. *Physiol. Genomics* **16**, 349–360 (2004).
29. Perrino, C. *et al.* Intermittent pressure overload triggers hypertrophy-independent cardiac dysfunction and vascular rarefaction. *J. Clin. Invest.* **116**, 1547–1560 (2006).
30. Spindler, M. *et al.* Diastolic dysfunction and altered energetics in the alphaMHC403/+ mouse model of familial hypertrophic cardiomyopathy. *J. Clin. Invest.* **101**, 1775–1783 (1998).
31. Sugimoto, H., Mundel, T.M., Kieran, M.W. & Kalluri, R. Identification of fibroblast heterogeneity in the tumor microenvironment. *Cancer Biol. Ther.* **5**, 1640–1646 (2006).
32. Mandelbrot, D.A. *et al.* B7-dependent T-cell costimulation in mice lacking CD28 and CTLA4. *J. Clin. Invest.* **107**, 881–887 (2001).
33. Lefer, A.M., Tsao, P.S., Ma, X.L. & Sampath, T.K. Anti-ischaemic and endothelial protective actions of recombinant human osteogenic protein (hOP-1). *J. Mol. Cell. Cardiol.* **24**, 585–593 (1992).
34. Gould, S.E., Day, M., Jones, S.S. & Dorai, H. BMP-7 regulates chemokine, cytokine, and hemodynamic gene expression in proximal tubule cells. *Kidney Int.* **61**, 51–60 (2002).
35. Nicoletti, A. & Michel, J.B. Cardiac fibrosis and inflammation: interaction with hemodynamic and hormonal factors. *Cardiovasc. Res.* **41**, 532–543 (1999).
36. McMullen, J.R. *et al.* Phosphoinositide 3-kinase(p110alpha) plays a critical role for the induction of physiological, but not pathological, cardiac hypertrophy. *Proc. Natl. Acad. Sci. USA* **100**, 12355–12360 (2003).
37. Villarreal, F.J. & Dillmann, W.H. Cardiac hypertrophy-induced changes in mRNA levels for TGF-beta 1, fibronectin, and collagen. *Am. J. Physiol.* **262**, H1861–H1866 (1992).
38. Tomita, H. *et al.* Early induction of transforming growth factor-beta via angiotensin II type 1 receptors contributes to cardiac fibrosis induced by long-term blockade of nitric oxide synthesis in rats. *Hypertension* **32**, 273–279 (1998).
39. Zeisberg, M. *et al.* Bone morphogenic protein-7 inhibits progression of chronic renal fibrosis associated with two genetic mouse models. *Am. J. Physiol. Renal Physiol.* **285**, F1060–F1067 (2003).
40. Lips, D.J. *et al.* Left ventricular pressure-volume measurements in mice: comparison of closed-chest versus open-chest approach. *Basic Res. Cardiol.* **99**, 351–359 (2004).

41. Sugimoto, H. *et al.* Bone-marrow-derived stem cells repair basement membrane collagen defects and reverse genetic kidney disease. *Proc. Natl. Acad. Sci. USA* **103**, 7321–7326 (2006).
42. Lyden, D. *et al.* Impaired recruitment of bone-marrow-derived endothelial and hematopoietic precursor cells blocks tumor angiogenesis and growth. *Nat. Med.* **7**, 1194–1201 (2001).
43. Takemoto, M. *et al.* Chronic angiotensin-converting enzyme inhibition and angiotensin II type 1 receptor blockade: effects on cardiovascular remodeling in rats induced by the long-term blockade of nitric oxide synthesis. *Hypertension* **30**, 1621–1627 (1997).
44. Razeghi, P. *et al.* Lack of NF-kappaB1 (p105/p50) attenuates unloading-induced downregulation of PPARalpha and PPARalpha-regulated gene expression in rodent heart. *Cardiovasc. Res.* **74**, 133–139 (2007).
45. Zeisberg, M. *et al.* BMP-7 counteracts TGF-beta1-induced epithelial-to-mesenchymal transition and reverses chronic renal injury. *Nat. Med.* **9**, 964–968 (2003).
46. Zeisberg, E.M. *et al.* Morphogenesis of the right ventricle requires myocardial expression of Gata4. *J. Clin. Invest.* **115**, 1522–1531 (2005).
47. Maeshima, Y. *et al.* Identification of the anti-angiogenic site within vascular basement membrane derived tumstatin. *J. Biol. Chem.* **7**, 7 (2001).
48. Maresh, J.G., Xu, H., Jiang, N. & Shohet, R.V. In vivo transcriptional response of cardiac endothelium to lipopolysaccharide. *Arterioscler. Thromb. Vasc. Biol.* **24**, 1836–1841 (2004).
49. Steidl, U. *et al.* Essential role of Jun family transcription factors in PU.1 knockdown-induced leukemic stem cells. *Nat. Genet.* **38**, 1269–1277 (2006).
50. Okuno, Y. *et al.* Distal elements are critical for human CD34 expression in vivo. *Blood* **100**, 4420–4426 (2002).